Semiconductor Physics, Quantum Electronics & Optoelectronics, 2011. V. 14, N 2. P. 137-144.

PACS 73.50.Td, 85.30.Kk

Dynamic properties and avalanche noise analysis of 4H-SiC over wz-GaN based IMPATTs at mm-wave window frequency

P.R. Tripathy[1], Moumita Mukherjee[2] and S.P. Pati[3]
[1]*Purushottam Institute of Engineering & Technology, Rourkela, Odisha, India*
[2]*CMSDS, Institute of Radio Physics & Electronics, University of Calcutta*
1, Girish Vidyaratna Lane, Kolkata 700009, West Bengal, India
[3]*National Institute of Science & Technology, Berhampur, Odisha, India*
[1,3]*School of Physics, Sambalpur University, Sambalpur, Odisha, India*
E-mail: pravashrt76@yahoo.co.in, mm_drdo@yahoo.com, prof_sppati@yahoo.co.in

Abstract. The mm-wave as well as noise properties of IMPATT diodes for the D-band are efficiently determined, with 4H-SiC and wurtzite type GaN as base materials, using advanced computer simulation techniques developed by the authors. The breakdown voltage (180 V) and efficiency (14.7%) is higher in case of 4H-SiC as compared to wz-GaN based diode having the breakdown voltage (153 V) and efficiency (13.7%). The study indicates that 4H-SiC IMPATT diode is capable of generating high RF power density of about 8.383×10^{10} W/m^2 as compared to GaN IMPATT diode that is capable to develop the power density 6.847×10^{10} W/m^2 for the same frequency of operation. It is also observed that wz-GaN exhibits better noise behavior 7.42×10^{-16} V^2·s than SiC (5.16×10^{-15} V^2·s) for IMPATT operation at 140 GHz. A tradeoff between the power output and noise from the device reveals that wz-GaN would be a suitable base material for high power application of IMPATT diode with moderate noise.

Keywords: avalanche noise, gallium nitride, IMPATT, RF power, silicon carbide, mm-wave window frequency.

Manuscript received 15.06.10; accepted for publication 16.03.11; published online 30.06.11.

1. Introduction

IMPATT diodes has been identified as a premier class of semiconductor devices suitable for stable RF power generation, used for present day e-communication systems with the added advantage that any form of *p-n* junction fabricated from any semiconductor material, can exhibit IMPATT action based on combined physical phenomena of both transit time and avalanche phase delay. Studies on new materials are being carried out by several groups spreading over the globe to enhance the RF power/efficiency and reduce the avalanche noise in this class of devices even at far mm-wave frequencies. In recent years, wide band gap materials like SiC and GaN, with their superior electronic properties, are studied for IMPATT action and the characteristics include high breakdown voltages, ability to sustain large electric fields, high temperature and high power applications as compared to the conventional narrow band gap Si-based IMPATT diode. The important and most attractive material for high power device applications is GaN and some of the various polytypes of SiC. In both these materials, the breakdown electric field strengths are expected to be about four times larger than corresponding values of narrow band gap material like Si or GaAs [1]. In addition, the other properties of GaN like wide energy band gap, high carrier saturation velocity and relatively small dielectric constants make them suitable for high power, high frequency amplifiers. GaN is emerging as an important semiconductor material for many diverse optoelectronics and electronics device applications [2, 3]. The wide direct band gap of GaN is particularly useful in short wavelength optoelectronic device applications. GaN is mostly grown in the wurtzite phase [4]. The 4H polytype, however, is considered as more appropriate for fabricating 4H-SiC IMPATT diodes due to higher and nearly isotropic electron mobility [5, 6]. Many reports suggest that IMPATT diodes based on these materials (GaN and 4H-SiC) are soon likely to find their place in modern communication systems. Thus, it has motivated the authors to undertake a comparative study on the

7

© 2011, V. Lashkaryov Institute of Semiconductor Physics, National Academy of Sciences of Ukraine

performance of IMPATT diodes based on these materials. The purpose of this work is to characterize the performances of the double drift IMPATT diodes with SiC and GaN as base materials, for application in D-band. The simulation method has been made sensible by incorporating most recently reported material parameters data for SiC and GaN [7, 8]. The mm-wave as well as noise properties of IMPATT diodes in D-band are efficiently computed, with 4H-SiC and wz-GaN as base materials, using our computer simulation scheme. The results are quite helpful in determining the best suited material for IMPATT operation at 140 GHz.

2. Computer simulation method

The three-stage computer simulation method consists of DC analysis, small signal analysis and noise analysis. The equations involved in these analyses are nonlinear in nature, and thus their solution involves complexity. So, we have first considered the diode to be consisting of small space points. The diode active layer width is divided into several number of space points with a space step of 0.1 nm. Fig. 1 represents the schematic structure of a double drift IMPATT diode.

2.1. DC analysis

The DC analysis is done by solving simultaneously three non-linear device equations, namely: Poisson's equation, the carrier continuity equation and the space charge equation using a double iterative field extremism initiated using DC simulation program [9]. The DC electric field profiles, carrier current profiles, breakdown voltage, etc., are obtained from this analysis. The ionization rates of electrons and holes for both these materials have been taken from the recent experimental reports for 4H-SiC [10] and wz-GaN [11, 12],

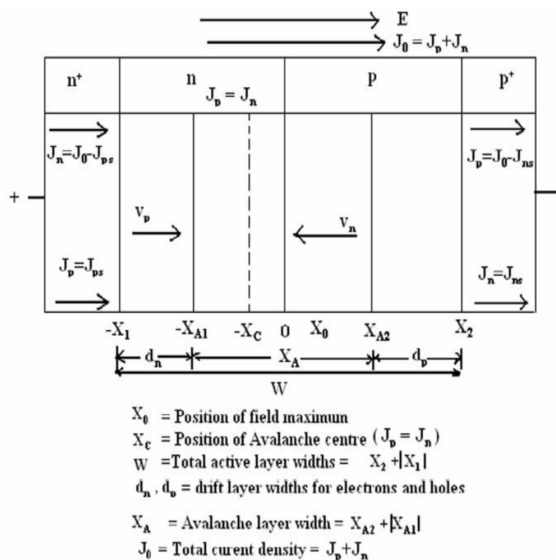

Fig. 1. Active layer of a double drift IMPATT diode.

respectively. The computer method framed for DC analysis is initiated from the location of the field maximum point E_0 at $x = x_0$ within the *p-n* junction, where $\frac{\partial E}{\partial x} = 0$, the value of the field maximum E_0 and its location x_0 are suitably chosen for the diode, and then it is used to obtain the value of the mobile space charge $\varphi(x_0)$ at the starting point. Then the Poisson equation and the carrier continuity equations are solved simultaneously through the numerical approach [9]. Iterations over E_0 and x_0 are carried out till boundary conditions are satisfied at both edges of the depletion layer. The space step width is taken to be very small, i.e. of the order of 0.1 nm. The numerical solution is progressed from the point $x = x_0$ and moving first towards the right side of the field maximum till the field boundary condition, in carrier current and electric field is satisfied at $x = x_R$. Thus, the DC field and carrier current distribution profiles for a particular IMPATT diode operating at a given current density are obtained from the final solution of E_0 and x_0. The method described above gives the avalanche breakdown characteristics of the IMPATT diode. The depletion layer width of the diode is obtained as $W = |x_L| + |x_R|$. The avalanche layer width x_A can be determined from the condition $|P(x)| = 0.95$, i.e. 95% growth of carrier current. The drift zone width is then obtained from the expression $(W - x_A)$. The voltage drop across different zones, i.e. breakdown voltage (V_B) and avalanche voltage drop (V_A) are determined by integrating the electric field over the respective zone layer. The drift voltage drop is then taken as $V_D = V_B - V_A$. The qualitative value of diode efficiency (η) can be obtained from the expression $\eta = V_D / \prod V_B$. The DC electric field profiles, carrier current profiles, breakdown voltage, etc., are obtained from this analysis. We have considered a one dimensional model with doping distributions of the form n^+-n-p-p^+. The data obtained from the DC analysis are used as input for the high frequency analysis of the diode.

2.2. Small signal analysis

The high frequency analysis of the diode is carried out using the small signal simulation method developed by our group [13]. The small signal model takes into account the contribution from each space point and effectively determines the device parameters such as negative conductance ($-G$), susceptance (B) and negative resistance ($-Z_R$) of the diode. The variations of these values with frequency are also computed using the double iterative computer program [12]. In the high frequency analysis, it is possible to find out the spatial variation of negative resistance (R) and reactance (X) in the depletion layer, which would provide a clear idea regarding the intensity of microwave oscillation along different regions of the diode. The unperturbed diode impedance Z_0 (without considering the diffusion current)

© 2011, V. Lashkaryov Institute of Semiconductor Physics, National Academy of Sciences of Ukraine

is separated into its real and imaginary components (i.e. $Z_0 = R_0 + iX_0$) to obtain the second order non-linear implicit differential equation in small signal resistance (R_0) and reactance (X_0) as

$$\frac{\partial^2 R_0}{\partial x^2} + (\alpha_n - \alpha_p)\frac{\partial R_0}{\partial x} - \frac{2r_-\omega}{\bar{v}}\frac{\partial X_0}{\partial x} + \left[\frac{\omega^2}{\bar{v}^2} - H(x)\right]R_0 - \frac{2\bar{\alpha}\omega}{\bar{v}}X_0 = \frac{2\bar{\alpha}}{\bar{\alpha}\varepsilon}, \quad (1)$$

$$\frac{\partial^2 X_0}{\partial x^2} + (\alpha_n - \alpha_p)\frac{\partial X_0}{\partial x} - \frac{2r_-\omega}{\bar{v}}\frac{\partial R_0}{\partial x} + \left[\frac{\omega^2}{\bar{v}^2} - H(x)\right]X_0 + \frac{2\bar{\alpha}\omega}{\bar{v}}R_0 = -\frac{\omega}{\bar{v}^2\varepsilon}, \quad (2)$$

with

$$H(x) = \frac{2j}{\bar{v}\varepsilon}\frac{\partial\bar{\alpha}}{\partial E} + \frac{qr_+}{\bar{v}\varepsilon}\frac{\partial}{\partial E}\left[g_{Tn}(x) + g_{Tp}(x')\right] + \frac{\partial}{\partial E}(\alpha_p - \alpha_n)\frac{\partial E_m}{\partial x}.$$

Finally, the small signal diode resistance (R) and reactance (X) due to drift, diffusion and tunnel currents are obtained from the expression including a perturbation part

$$R = R_0 + \sum_k R_k \text{ and } X = X_0 + \sum_k X_k . \quad (3)$$

The integrated values of resistance and reactance give Z_R and Z_X, if using the relation,

$$Z_R = \int_0^W R(x)dx \text{ and } Z_x = \int_0^W X(x)dx . \quad (4)$$

Using the values of Z_R and Z_X, the diode conductance (G), susceptance (B) and the quality factor (Q) are calculated via the relations

$$G = \frac{Z_R}{Z_R^2 + Z_x^2}, \quad B = \frac{-Z_x}{Z_R^2 + Z_x^2} \text{ and } Q = -\left|\frac{B}{G}\right|. \quad (5)$$

The series positive resistance (R_S) of any device which is one of the important limiting factors responsible for limiting power output and device efficiency can also be determined. The expected RF power delivery from the diode can be computed using the relation

$$P_{RF} = (V_{RF})^2 |G_p| \times A/2. \quad (6)$$

The power density P_A is taken as P_{RF}/A, where A is the area of cross section of the device. V_{RF} can be approximated as $V_B/2$ for 50% modulation. G_p is the device negative conductance at the peak frequency [14].

2.3. Small signal noise analysis

The fundamental avalanching process involved in the IMPATT diode operation leads to sufficient avalanche noise generation in the device. So, noise is an important aspect of the present study and the noise characteristics of the diode structure are also computed using the generalized noise simulation program [15]. The noise characteristics like mean square noise voltage per bandwidth ($\langle V^2\rangle / \Delta f$) and noise measure (NM) of the device are computed from this analysis. The noise generation rate of individual sources can be calculated by using the equation:

$$\gamma_N(x') = n(x')\alpha_n(x')v_n(x') + p(x')\alpha_p(x')v_p(x'). \quad (7)$$

The exact values of n, p, α_n and α_p are determined from a static analysis of the diode under avalanche breakdown condition, which also gives the distribution of electric field and the carrier concentration along the depletion layer of the diode [16].

The noise sources $\alpha_n(x')$ are located at x' in the avalanche region gives rise to noise electric fields (x, x') at every point in the depletion region of the diode. The noise electric field ($e(x, x') = e_R(x, x') + i\, e_X(x, x')$) contribution from each space point is calculated using a double iterative simulation program [8], which solves the following two second-order differential equations for the real $e_R(x, x')$ and imaginary $e_X(x, x')$ parts of the noise electric field at each space point subject to the boundary conditions:

$$\frac{\partial^2 e_R}{\partial x^2} + (\alpha_n - \alpha_p)\frac{\partial e_R}{\partial x} - \frac{2r_-\omega}{\bar{v}}\frac{\partial e_X}{\partial x} + \left(\frac{\omega^2}{\bar{v}^2} - H\right)e_R - \frac{2\bar{\alpha}\omega}{\bar{v}}e_X = \frac{2r_+q\gamma_N}{\bar{v}\varepsilon} \quad (8)$$

and

$$\frac{\partial^2 e_X}{\partial x^2} + (\alpha_n - \alpha_p)\frac{\partial e_X}{\partial x} - \frac{2r_-\omega}{\bar{v}}\frac{\partial e_R}{\partial x} + \left(\frac{\omega^2}{\bar{v}^2} - H\right)e_X + \frac{2\bar{\alpha}\omega}{\bar{v}}e_R = 0. \quad (9)$$

First, the noise generation source is assumed to be located at the left-hand edge of the active zone at x'_i, where $i = 1$. Iterations over initial chosen values of e_R and e_X in the left-hand edge of the diode depletion layer are carried out till the boundary conditions are satisfied at the right-hand edge. The profiles of noise field e_R and e_X can be obtained from the final solution of equations (8) and (9). The method is repeated to obtain the integrated noise voltage and noise-field profile due to noise source successively located at $x = x' + n\,\partial x'$, where $n = 1, 2, 3, \ldots, 1000$. Thus, the noise generation profile along the length of the depletion layer can be determined separately for noise sources located in various space points of the active zone. The integrated values of $e_R(x, x')$ and $e_X(x, x')$ over x give the real and imaginary parts of the terminal voltage $V_R(x')$ and $V_X(x')$ due to noise generating source at x' and are obtained as

© 2011, V. Lashkaryov Institute of Semiconductor Physics, National Academy of Sciences of Ukraine

$$V_R(x') = \int_0^W e_R(x,x')dx \quad \text{and} \quad V_X(x') = \int_0^W e_X(x,x')dx . \quad (10)$$

The noise source is then shifted to $x = x_i'$ for $i = 2, 3,\ldots, n$ and $V_R(x')$, $V_X(x')$ are determined for individual noise sources. These values of $V_R(x')$ and $V_X(x')$ are then integrated for noise sources considered along the entire depletion zone.

So $V_R = \int_0^W V_R(x')dx'$ and $V_X = \int_0^W V_X(x')dx'$. (11)

These final values of V_R and V_X are taken to calculate the integrated noise parameters.

Now the diode transfer impedance (Z_T) can be computed taking the values of the terminal voltage from the equation (10). The transfer impedance of the diode is defined as the ratio of open circuit incremental voltage to the injected current at x'. Taking the injected current in x' as $dI_N = q\gamma_N(x')Adx'$, A being the area of cross section, one can obtain the real and imaginary parts of the transfer impedance using the relations

$$Z_{TR}(x') = \frac{V_R(x')}{q\gamma_N(x')Adx'} \quad \text{and}$$

$$Z_{TX}(x') = \frac{V_X(x')}{q\gamma_N(x')Adx'} . \quad (12)$$

The transfer impedance is determined from the relation

$$|Z_T(x',\omega)| = |Z_{TR}(x')|^2 + |Z_{TX}(x')|^2 . \quad (13)$$

Considering $q\gamma_N Adx'$ as a shot current fluctuation due to avalanching process and using the theory of shot noise, one can write the mean square deviation for the current as

$$\langle dI_N^2 \rangle = 2q\, dI_N \Delta f . \quad (14)$$

Using the expression for diode transfer impedance from the equation (13) and mean square fluctuation of current from the equation (14), one can compute the mean square noise voltage from the relation

$$\langle V^2 \rangle = 2q\Delta f \int |Z_T(x',\omega)|^2 \, q\gamma_N Adx'$$

$$\Rightarrow \frac{\langle V^2 \rangle}{\Delta f} = 2q^2 A\gamma_N \int |Z_T(x',\omega)|^2 \, dx' . \quad (15)$$

From the knowledge of the mean square noise voltage, the noise measure (NM) of the diode can be computed from the expression

$$\text{NM} = \frac{\langle V^2 \rangle / \Delta f}{4KT(-Z_R)} , \quad (16)$$

where K is the Boltzmann constant, T is the junction temperature (taken to be 473 K) and $-Z_R$ is the total negative diode resistance.

3. Results and discussion

3.1. Comparison of GaN and SiC-based IMPATTs: simulation results

The results obtained from the computer simulation for IMPATT diodes, with 4H-SiC and wz-GaN as base materials, are presented in this section. The breakdown voltage (V_B) for 4H-SiC IMPATT diode is found to be 180 V and that for GaN IMPATT diode is 153 V. The breakdown electric field has been computed to be 5.33×10^8 V/m for wz-GaN as compared to 7.30×10^8 V/m for 4H-SiC based IMPATT diode. High breakdown field results in a high breakdown voltage. It is worth to mention here that these values of the breakdown voltage are approximately 10-12 times higher than the corresponding values of the breakdown voltage for Si IMPATT diodes designed to operate at the same frequency (13.3 V for 140 GHz). Since the breakdown voltage is indicative of input power of the device, 4H-SiC and wz-GaN are promising IMPATT diode materials for high-power operation.

Material and physical parameters of both these materials, i.e. 4H-SiC and wz-GaN, are presented in Table 1. The other device properties like device negative conductance, expected power density, mean square noise voltage per bandwidth, etc., at 140 GHz are presented in Table 2. Fig. 2 shows the electric field profile for both materials (4H-SiC and wz-GaN) based DD IMPATTs. The variation of the negative conductance with frequency for 4H-SiC and GaN IMPATT diodes are plotted in Fig. 3. The variation of the power density versus frequency is also plotted in Fig. 4. The negative conductance for both 4H-SiC and wz-GaN diodes peaks at around 140 GHz which can be regarded as an optimum frequency of operation of the diodes. The negative resistance contribution at any space step, which is the ratio of ac voltage (eac) to ac current(iac), can be computed from the final computer run as the magnitude of R0 in the corresponding space step. It is seen that the negative resistance profile along depletion zone is of double peak nature with one peak remaining in each of the drift region. The peak of negative resistance together with its spread along the active zones indicates contribution of negative resistance by individual space step. However, in case of both the diodes, the avalanche zones produce positive RF resistance. The magnitude of the peak for the negative resistance profile is higher in 4H-SiC diode than that for wz-GaN diode. This leads to higher RF power generation from 4H-SiC device. These facts are reflected from Table 2 and Fig. 4, which indicates that 4H-SiC DDR shows high power density and, thus, 4H-SiC may have an advantage for being chosen as a base material for IMPATT diodes.

In order to make a comparison, the authors have also studied the properties of silicon IMPATT DDR for the same frequency of 140 GHz. The power density from silicon diode remains only around 3.274×10^9 W/m^2, which is nearly lower by a factor of around 25 than its SiC and GaN counterparts. However, wz-GaN has the

© 2011, V. Lashkaryov Institute of Semiconductor Physics, National Academy of Sciences of Ukraine

advantage of producing low noise as compared to 4H-SiC for IMPATT operation at 140 GHz. This can be inferred from Fig. 5 where the authors have plotted the variation of mean square noise voltage per band width versus frequency for IMPATT diodes based on these two materials. This graph shows the transition frequency where the plots show peak. However, the mean noise square voltage at around 140 GHz is lower for GaN diode. The noise measure has been presented in Fig. 6 for both materials also reflect the same fact. Basing on a tradeoff between the power output and noise from the device, it reveals that wz-GaN would be a suitable base material for high power application of IMPATT diodes with moderate noise.

Table 1. Material parameters of 4H-SiC and wz-GaN.

Parameter	4H-SiC	wz-GaN
Band gap, E_g (eV)	3.26	3.45
Dielectric constant, ε_r	10.1	9.0
Critical electric field, E_c ($\times 10^7$ V/m)	35.0	30.0
Thermal conductivity, θ (W/m·K)	500.0	225.0
Electron mobility, μ_e (cm^2/v·s)	1140	1600
Hole mobility, μ_h (cm^2/v·s)	50	28
Saturated electron drift velocity, v_{sat} ($\times 10^5$ m/s)	2.0	2.5

Table 2. mm-wave and noise properties of IMPATT diodes with 4H-SiC and wz-GaN as base materials, designed for operation at 140 GHz.

Parameter	4H-SiC	wz-GaN
Break down voltage (V_B)	180	153
Efficiency (η) (%)	14.7	13.7
Negative conductance, $-G$ (S/m^2)	2.07×10^7	2.34×10^7
Power density (W/m^2)	8.383×10^{10}	6.847×10^{10}
$\langle V^2\rangle/\Delta f$ (V^{2}s)	5.16×10^{-15}	7.42×10^{-16}
Noise measure (dB)	36.1	31.8

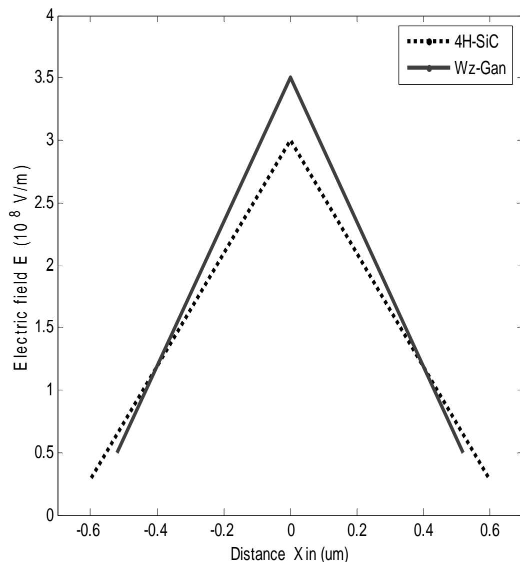

Fig. 2. Electric field profiles for 4H-SiC and wz-GaN DD IMPATT.

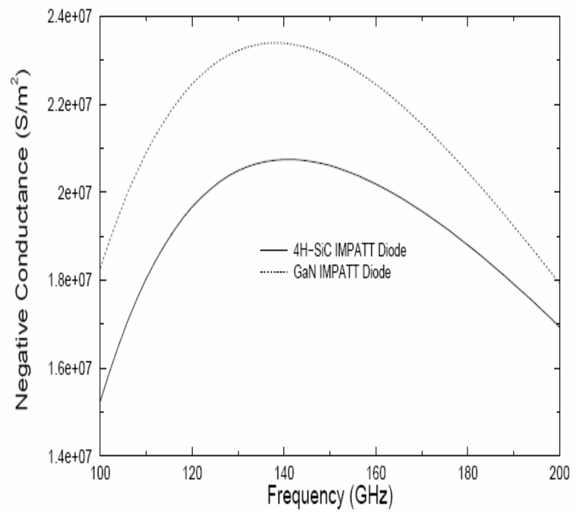

Fig. 3. Variation of the negative conductance with frequency for 4H-SiC and GaN IMPATT diodes.

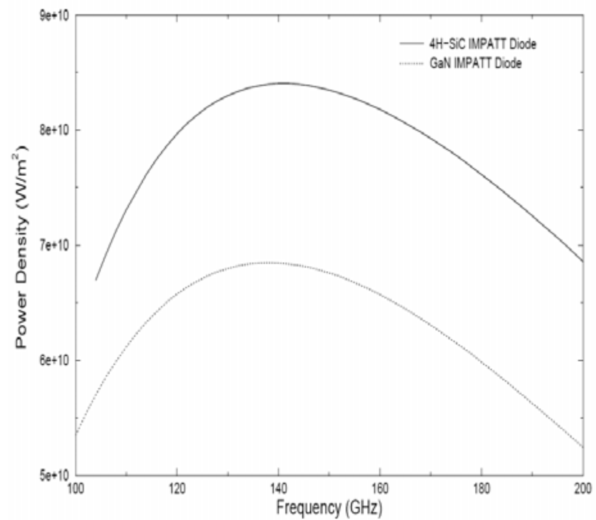

Fig. 4. Variation of the power density with frequency for 4H-SiC and GaN IMPATT diodes.

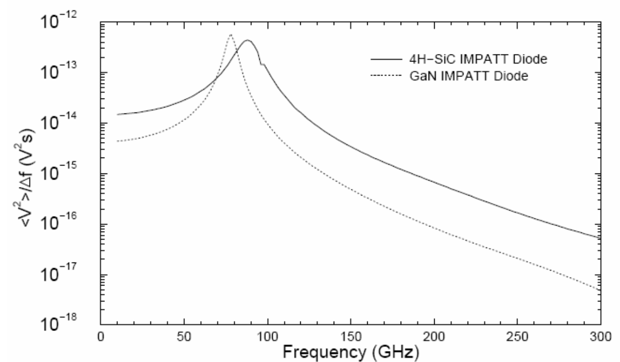

Fig. 5. Variation of the mean square noise voltage per bandwidth with frequency for 4H-SiC and GaN IMPATT diodes.

© 2011, V. Lashkaryov Institute of Semiconductor Physics, National Academy of Sciences of Ukraine

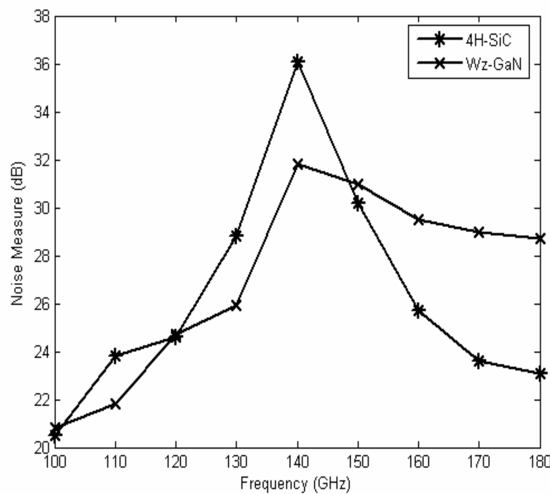

Fig. 6. Noise measure versus frequency for wz-GaN and 4H-SiC DDRs.

3.2. Fabrication issue related to GaN and SiC-based IMPATT diodes

The computer simulation results show the importance and superiority of both the wide band gap material (4H-SiC and wz-GaN) for high-power source at mm-wave regime. Special efforts have been taken for the material growth, doping and device processing, oscillator performance, characterization of the device by taking the SiC and GaN as base material for fabrication of the diode [17, 18]. Due to the lack of experimental data on wide band gap semiconductor mm-wave devices, simulation results could not be compared. However, the authors have proposed the practical issues related to the fabrication of GaN and SiC IMPATT devices. GaN *p-n* junction can be obtained by using the molecular beam epitaxy (MBE). In order to form an *p-n* junction, first, the MBE growth process can be carried out using Si donor impurity to form the *n*-type layer of GaN on an n^+ substrate, and after that, a p^+-type cap layer can be grown on the *n*-layer by the MBE process by doping high concentration of Mg impurity. In order to activate *p*-type conductivity, high-temperature post-growth anneal in a nitrogen atmosphere may be required. Because Mg requires large energy for ionization, in general, it is difficult to obtain heavily doped p^+-type GaN with Mg. Beryllium (Be) may be used to achieve p^+-type GaN because the ionization energy of Be is low (~60 meV). Recently, Pastor et al. [19] assessed the crystal damage of Be^+-implanted GaN by UV Raman scattering and found a correlation between implantation dose and the extent of lattice damage caused to the target.

A SiC IMPATT device can be fabricated on the epiwafer by following the process steps briefly described below [20].

Growth of p^+ 4H-SiC layer

In order to assist *p*-type ohmic contact formation, the p^+ 4H-SiC layer can be grown on the top of *n*-type film by Al^{2+} ion implantation. The post-implantation annealing may be performed at a very high temperature in an argon atmosphere.

Formation of low-resistive p^+ and n^+ contacts

Power dissipation of IMPATT devices strongly depends on the contact resistance. The samples may be cleaned by a "piranha" solution. After rinsing in DI water, the

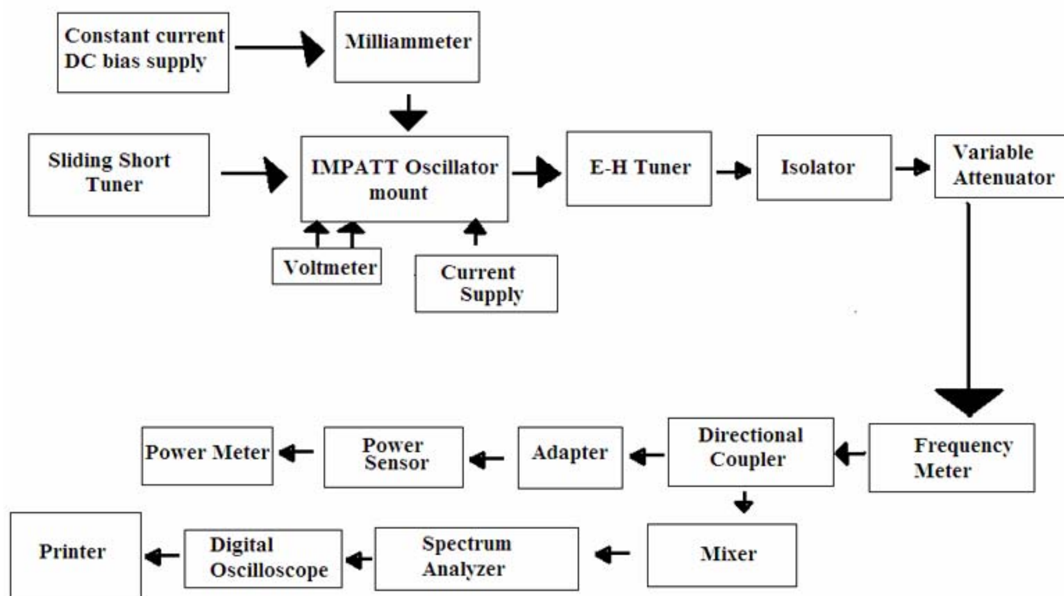

Fig. 7. Experimental arrangement for realization of SiC and GaN IMPATT diodes for D-band.

© 2011, V. Lashkaryov Institute of Semiconductor Physics, National Academy of Sciences of Ukraine

samples may be dipped in dilute hydrofluoric acid solution and dried for nearly fifteen minutes. Through the lithographic process, windows can be opened inside the oxide layer. Using lithography and liftoff techniques, contact metals (Al/Ti/Al) can then be deposited in the oxide windows by an electron beam evaporator. In order to obtain ohmic contacts, the samples may be annealed for 3 to 5 min in a rapid thermal anneal (RTA) furnace in nitrogen atmosphere at around 950 °C. The post-deposition annealing at high temperature is generally preferred to reduce the specific contact resistance. For an n^+-type contact, an Ni layer of 200-nm thickness may be evaporated on the backside (n^+-side) of the wafer, followed by the RTA treatment for 3 min at 950 °C [21]. The choice of the metallic composition is based on the formation of Ni_2Si alloy. As mentioned in several publications [22], the higher the concentration of Ni_2Si in contacts is, the lower the specific contact resistance is. The specific contact resistance can be determined from transmission line measurement (TLM) data. Several experimental attempts have been taken for the development of SiC material for device fabrication [23-25].

Experimental verification of mm-wave properties of IMPATT diodes can be done by the arrangement shown in Fig. 7 [26].

4. Conclusion

A detailed comparative analysis of both 4H-SiC and wz-GaN-based IMPATT devices in the millimeter-wave range has been reported by studying the DC, small signal and avalanche noise analysis through the simulation technique developed by the authors. It may be concluded that both 4H-SiC and GaN are potential materials for high power IMPATT application. The wide gap associated with a high breakdown voltage in both cases with tolerance to the high operating current density would help in possible realization of high RF power. Both 4H-SiC and GaN diodes may yield a RF power 25-30 times higher than its Si counterpart. It is observed that for high-power operation the 4H-SiC is a suitable base material for IMPATT diode, whereas GaN is a better material than SiC for high power operation with moderate noise. To the best of authors' knowledge this is the first report on the comparative analysis of mm-wave characteristics and avalanche noise analysis of SiC and GaN IMPATTs at an important window frequency of 140 GHz. This study will be useful for practical realization of high-power, low noise IMPATT in the mm-wave region.

Acknowledgement

Moumita Mukherjee is grateful to Defence Research and Development Organisation, Ministry of Defence, Govt. of India for providing her 'Senior Research Fellowship' to carry out this research work.

References

1. V.V. Buniatyan and V.M. Aroutiounian, Wide gap semiconductor microwave devices // *J. Phys. D: Appl. Phys.,* **40** (20), p. 6355-6385 (2007).
2. M.S. Shur, GaN based transistors for high power applications // *Solid-State Electron.*, **42**(12), p. 2131-2138 (1998).
3. U.K. Mishra, Y. Wu, B.P. Kellar, S. Kelar, S.P. Baars Den, GaN microwave electronics // *IEEE Trans. Microwave Theory Technique* **MTT-46**, p. 756-761 (1999).
4. S.J. Peatron, J.C. Zolper, R.J. Shul and F. Ren, GaN: processing, defects, and devices // *J. Appl. Phys.* **86**, p. 1-78 (1999).
5. J.B. Casady and R.W. Johnson, Status of silicon carbide as a wide-bandgap semiconductor for high-temperature applications: a review // *Solid-State Electron.*, **39**(10), p. 1409-1422 (1996).
6. P.G. Neudeck, Progress in silicon carbide semiconductor electronics technology // *J. Electron. Mater.*, **24** (4), p. 283-288 (1995).
7. W.S. Loh, B.K. Ng, J.S. Ng, Stanislav I. Soloviev, Ho-young Cha, Peter M. Sandvik, C. Mark Johnson and John P.R. David, Impact ionization coefficients in 4H-SiC // *IEEE Trans. Electron. Devices*, **55**(8), p. 1984-1990 (2008).
8. A. Reklaitis and L. Reggiani, Monte Carlo study of hot-carrier transport in bulk wurtzite GaN and modeling of a near-terahertz impact avalanche transit time diode // *J. Appl. Phys.,* **95**(12), p. 7925-7935 (2004).
9. P.R. Tripathy, A.K. Panda and S.P. Pati, Comparison between the DC and microwave performance of wurtzite phase and zinc-blende phase GaN-based IMPATTs // *Proc. XV Intern. Workshop on Physics of Semiconductor Devices* (IWPSD-2009), p. 525-528 (2009).
10. Electronic Archive: New Semiconductor Materials, Characteristics and Properties. [Online]. Available: *http://www.ioffe.rssi.ru/SVA/NSM/Semicond/SiC*
11. I.H. Oguzman, E. Belloti, K.F. Brennan, J. Kolnik, R. Wang, P.P. Buden, Theory of hole initiated impact ionization in bulk zinc blende and wurtzite GaN // *J. Appl. Phys.*, **81**(2), p. 7827-7836 (1997).
12. Electronic Archive: New Semiconductor Materials, Characteristics and Properties. [Online]. Available: *http://www.ioffe.rssi.ru/SVA/NSM/Semicond/GaN*
13. S.K. Dash and S.P. Pati, Effect of optical radiation on millimeter-wave characteristics and avalanche noise generation in double-drift IMPATT diodes based on opto-sensitive semiconductors // *Microwave and Optical Technology Letter*, **33**(4), p. 295-300 (2002).
14. H. Eisele and G.I. Haddad, *Microwave Semiconductor Device Physics*, S.M. Sze Ed. Willey, New York, 1997, p. 343.

© 2011, V. Lashkaryov Institute of Semiconductor Physics, National Academy of Sciences of Ukraine

15. A.K. Panda, D. Pavlidis, and E. Alekseev, Noise characteristics of GaN-based IMPATTs // *IEEE Trans. Electron Devices*, **48**, p. 1473-1475 (2001).
16. A. Reklaitis and L. Reggiani, Monte Carlo investigation of current voltage and avalanche noise in GaN double-drift impact diodes // *J. Appl. Phys.*, **97**, 043709 (2005).
17. K. Vassilevski, K. Zekentes, G. Constantidis, A. Strel'chuck, Fabrication and electrical characterization of 4H-SiC p^+-n-n^+ diodes with low differential resistance // *Solid-State Electron.*, **44**, p. 1173-1177 (2000).
18. S.J. Pearton, C.B. Vartuli, J.C. Zolper, C. Yuan, and R.A. Stall, Ion implantation doping and isolation of GaN // *Appl. Phys. Lett.*, **67**(10), p. 1435-1437 (1995).
19. D. Pastor, J. Ibáñez, R. Cuscó, L. Artús, G. González-Diaz, and E. Calleja, Crystal damage assessment of Be^+-implanted GaN by UV Raman scattering // *Semicond. Sci. Technol.*, **22**(2), p. 70-73 (2007).
20. M. Mukherjee, N. Mazumder and S.K. Roy, Photosensitivity analysis of gallium nitride and silicon carbide terahertz IMPATT oscillators: Comparison of theoretical reliability and study on experimental feasibility // *IEEE Trans. Device and Materials Reliability*, **8**, p. 608-620 (2008).
21. R. Konishi, R. Yasokuchi, O. Nakatsuka, Y. Koide, M. Moriyama, and M. Murakami, Development of Ni/Al and Ni/Ti/Al ohmic contact materials for p-type 4H-SiC // *Mater. Sci. Eng. B*, **98** (3), p. 286-293 (2003).
22. C.H. Carter Jr., V.F. Tsvetkov, R.C. Glass, D. Henshall, M. Brady, S.G. Muller, O. Kordina, K. Irvine, J.A. Edmond, H.-S. Kong, R. Singh, S.T. Allen, J.W. Palmour, Progress in SiC: from material growth to commercial device development // *Mater. Sci. Eng*., **B61-**2, p. 1-8 (1999).
23. R.R. Siergiej, R.C. Clarke, S. Sriram, A.K. Agarwal, R.J. Bojko, A.W. Morse, V. Balakrishna, M.F. MacMillan, A.A. Burk Jr., C.D. Brandt, Advances in SiC materials and devices: an industrial point of view // *Mater. Sci. Eng.* **B61-2**, p. 9-17 (1999).
24. R. Madar, Silicon carbide in contention // *Nature*, **430**, p. 1009-1012, Aug. 26 (2004).
25. L. Yuan, J.A. Cooper Jr, M.R. Melloch and K.J. Webb, Experimental determination of a SiC IMPATT oscillator // *IEEE Electron Device Lett.*, **22**(6), p. 266 (2001).
26. M. Mukherjee, N. Mazumder and A. Dasgupta, Simulation experiment on optical modulation of 4H-SiC millimeter-wave high power IMPATT oscillator // *J. Europ. Microwave Association (EuMA Publishing – UK)*, **4**, p. 276-282 (2008).

© 2011, V. Lashkaryov Institute of Semiconductor Physics, National Academy of Sciences of Ukraine